Measurement Science
and Technology

100 year anniversary
Measurement Science and Technology

PURPOSE-LED
PUBLISHING™

PAPER • **OPEN ACCESS**

Assessment of a space and energy resolved diagnostic based on GEM technology on MAST-U

To cite this article: A Celora *et al* 2025 *Meas. Sci. Technol.* **36** 016019

View the article online for updates and enhancements.

You may also like

- High-precision automated processing of sequential images for high-speed videogrammetric measurement
Xianglei Liu, Yuqi Zhang, Yuan Yao et al.
- Study on enhancing the quantitative performance of LIBS for Cu element in liquids based on the chitosan-parafilm enrichment method
Hongbao Wang, Honglian Li, Zhichao Yao et al.
- Differential evolution-based time domain decomposition method for multi-impact vibration signals of reciprocating machinery
Quanli Dou, Yedong Song, Zhenjing Zhang et al.

This content was downloaded from IP address 194.81.223.66 on 14/02/2025 at 15:19

OPEN ACCESS
IOP Publishing
Measurement Science and Technology
Meas. Sci. Technol. **36** (2025) 016019 (9pp)
https://doi.org/10.1088/1361-6501/ad8cfb

Assessment of a space and energy resolved diagnostic based on GEM technology on MAST-U

A Celora[1,2,*], F Caruggi[1,2,3], O Putignano[2,3], S Cancelli[1,2,3], G Claps[4,5], F Cordella[4,5], L Garzotti[6], G Gorini[1,2,3], G Grosso[3], F Guiotto[7,8], E Lazzaro[3], M Nocente[1,3], D Pacella[4,5], E Perelli Cippo[3], D Rigamonti[2,3], E Rose[6], R Sarwar[6], R Scannell[6], F Scioscioli[2,3], M Tardocchi[2,3], G Croci[1,2,3] and A Muraro[2,3]

[1] Dipartimento di Fisica 'G. Occhialini', University of Milano-Bicocca, Piazza della Scienza 3, Milano, Italy
[2] Istituto per la Scienza e Tecnologia dei Plasmi, CNR, via Cozzi 53, Milano, Italy
[3] INFN, Sezione Milano-Bicocca, Piazza della Scienza 3, Milano, Italy
[4] ENEA-Frascati, V. E. Fermi 44, Frascati, Italy
[5] INFN, Laboratori Nazionali di Frascati, via Enrico Fermi 40, Frascati, Italy
[6] UKAEA-CCFE, Culham Science Centre, Abingdon, Oxfordshire OX14 3DB, United Kingdom
[7] Centro Ricerche Fusione (CRF), University of Padova, Padova, Italy
[8] Consorzio RFX (CNR, ENEA, INFN, University of Padova, Acciaierie Venete SpA), C.so Stati Uniti 4, 35127 Padova, Italy

E-mail: a.celora@campus.unimib.it

Received 17 July 2024, revised 16 October 2024
Accepted for publication 30 October 2024
Published 11 November 2024

Abstract

A gas electron multiplier (GEM)-based detector was utilized for the first time on a spherical tokamak, MAST-U, during the 2023 campaign to investigate soft x-ray (SXR) radiation (1–20 keV) emitted from the plasma. GEM detectors, chosen for their resilience to harsh fusion environments and their ability to provide energy-resolved ($E_{res} \sim 25\%$ at 8 keV) SXR emission images (with a spatial resolution of few centimeters) with sub-millisecond time resolution, are a relatively new diagnostic compared to standard semiconductor diodes. In this study, the GEM detector features a pinhole geometry outside the vacuum chamber and observes the plasma through a beryllium window. Filled with an ArCO2 mixture, the detector consists of an Aluminized Mylar cathode, three Aluminum-coated GEM foils, and an anode made of a 16×16 matrix of 6 mm^2 pads for 2D readout. It employs custom GEMINI ASICs (Application Specific Integrated Circuits) for signal readout, enabling single photon-counting techniques with Time over Threshold analysis on each detector channel, for a maximum rate of 1 MHz per channel. Preliminary results from the 2023 campaign highlight the GEM detector's ability to complement existing SXR camera systems by adding energy-resolved information to the spatial and temporal data. Case studies demonstrate the detector's capability to capture Magnetohydrodynamic instabilities, such as Snake instabilities, while utilizing

* Author to whom any correspondence should be addressed.

Original Content from this work may be used under the terms of the Creative Commons Attribution 4.0 licence. Any further distribution of this work must maintain attribution to the author(s) and the title of the work, journal citation and DOI.

© 2024 The Author(s). Published by IOP Publishing Ltd

its energy-resolved measurements to analyze plasma events, including Internal Reconnection Events. Additionally, the GEM detector enables the estimation of Electron Temperature in Maxwellian plasmas from SXR measurements. These findings underscore the potential of the GEM-based diagnostic system to enhance the understanding of tokamak plasmas by providing simultaneous spatial, temporal, and energy-resolved insights.

Keywords: plasma diagnostic, gas electron multiplier, x-ray detectors, spherical tokamak

1. Introduction

The analysis of soft x-ray (SXR) radiation (1–20 keV) emitted by the plasma is a fundamental procedure in tokamak thermonuclear fusion experiments [1]. This radiation is closely linked to several local plasma parameters such as plasma density, electron temperature and pression, as it is mainly produced thorugh Bremmstrahlung processes [2]. Additionally, medium-to-heavy atom impurities contribute by emitting line radiation [3]. Thus SXR diagnostics provide essential insights into plasma phenomenology, facilitating the study of various physical processes including Magnetohydrodynamics instabilities, plasma disruptions, particle transport and impurity dynamics.

Semiconductor diodes have traditionally served as standard SXR detectors for tokamak applications but they face two primary limitations. Firstly, they are prone to deterioration under the intense neutron fluxes of tokamak experiments, a concern exacerbated by the higher neutron fluxes in next-generation tokamaks. Secondly, when employed as SXR diagnostics on tokamaks, they operate in current mode, not providing energy information. Consequently, the exploitation of gas electron multiplier (GEM) [4, 5] and scintillator-based detectors [6] has grown in the recent years. While the scintillators offer improved radiation hardness and excellent time resolution [7], GEM detectors can complement both technologies by adding energy-resolved analysis.

This work follows the series of installations of GEM detectors on several tokamaks such as FTU, KSTAR, EAST [8] and WEST [9]. It provides an overview of the first results from the exploitation of an aluminated GEM detector on MAST-U (Mega Ampere Spherical Tokamak Upgrade) [10] tokamak, highlighting the potential of such diagnostic on a spherical tokamak (ST) configuration. MAST-U features a medium-sized configuration with a major/minor radius of 0.7 m/0.5 m, a graphite first wall, and operates at a magnetic field strength of up to 0.7T. Employing high-performance plasma heating systems including neutral beam injection, MAST-U produces pulses typically lasting 1–2 s, with an electron density of 1.5×10^{19} m^{-3} and electron temperatures reaching up to 2.5 keV. Additionally, MAST-U is currently in the process of installing an electron heating system based on electron Bernstein wave . In this context, the energy resolution capabilities of the GEM camera could aid in studying the electron distribution function and assessing the possible necessity of other diagnostics.

1.1. The GEM detector

The detector utilized in this work is a type of micropattern gaseous detector based on the GEM foil technology. This type of detector operates based on the gaseous multiplication of photoelectrons generated by the interaction of incoming SXR radiation with the gas mixture, consisting of $70\% - 30\%$ $ArCO_2$. A GEM foil consists of a Kapton foil coated on both sides with metal, in this case Aluminum, and densely punctured. A potential difference is applied to both metallic sides that act as electrodes of the multiplication stage.

The detector, whose characterization is described in [11], consists of an aluminized mylar layer 10 nm–12 μm, serving as the cathode, followed by the active zone, called Drift region, three cascaded Al-GEM foils acting as multiplication stages, and finally, a padded Copper anode (the detector scheme is shown in figure 1(a), together with its geometrical parameters). The anode is composed by 16×16 6 mm^2 square pixels, to obtain a compact bidimensional camera of 10×10 cm^2, as shown in figure 1. The compact Readout electronics allow single photon counting functioning. It is composed by a set of 16 application specific integrated circuit called GEMINI [12], with 16 channels each, for a total of 256 read-out channels, and a custom made FPGA. Each pixel is read by a single GEMINI channel using the Time over Threshold technique, enabling retrieval of the time of the photoelectric interaction along with a signal proportional to the event energy. This signal is digitally converted into energy units through detector calibration [13]. Thus, the measurement is asynchronous and independent for each pixel, and the time binning can be adjusted for varying event rates, with a maximum event rate of 1 MHz per channel (and therefore pixel).

1.2. Experimental set up

The GEM camera is positioned outside of the outer wall of the tokamak vacuum chamber and is housed in an aluminum case (see figure 2), that acts as a Faraday cage, for safety and noise reduction purposes. It has a radial point of view (POV) of the plasma through a circular Beryllium window, 25 μm thick and 13 mm diameter. The case is approximately 30 cm from the window, which is 2.5 m from the tokamak center, therefore the SXR path traverses 30 cm of air. This means that the Argon present in air and the Beryllium window attenuate low-energy spectrum components, as shown in figure 7.

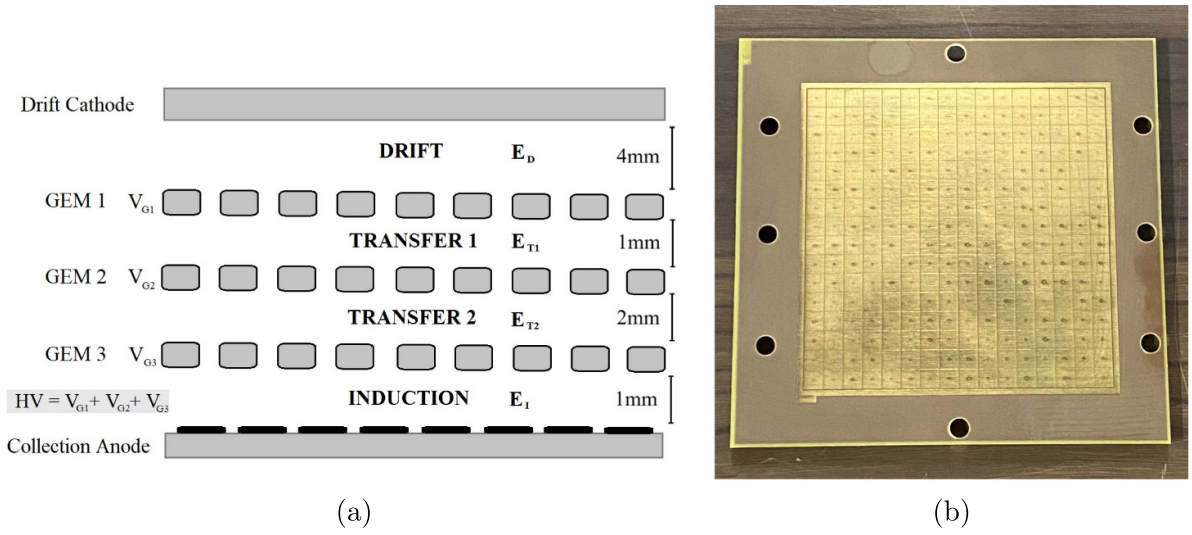

Figure 1. (a) Schematics of a triple-GEM detector [11]. (b) Picture of the 16 × 16 pixel detector anode.

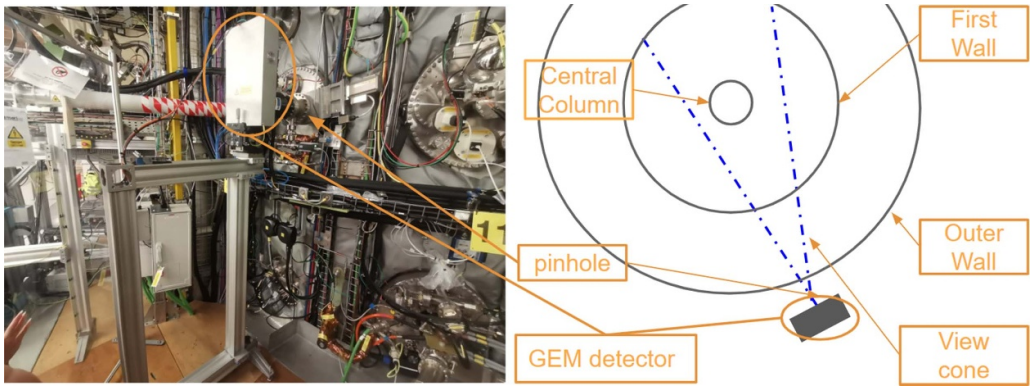

Figure 2. On the left: the GEM detector protective case installed on MAST-U. On the right: the top view of the GEM setup on MAST-U.

Prior to the Beryllium window, a gate valve is installed as a standard safety measure to maintain vacuum integrity in case of malfunctioning; it opens routinely during shot time to allow a direct view on the plasma, but can be kept closed, blocking the SXR radiation, to study signal background.

A centimeter after the Beryllium window is located an aperture, which is the system pinhole, with a diameter adjustable from 1 to 13 mm to optimize detector dynamic range, crucial for operation during both Ohmic and Beam heated shots. It should be noted that the GEM detector's bidimensionality, configured with a radial POV, enables integration over the rows of the pixel matrix to achieve the equivalent of a 1D horizontal camera, with a 16 MHz rate limit per row.

Remote control of the GEM foils voltage is achieved through an HV module [14], allowing adjustment of detector gain based on expected signal intensity to prevent signal saturation.

The SXR diode diagnostic setup on MAST-U includes multiple sets of pinhole SXR cameras, comprising both horizontal and vertical configurations. They serve for the purpose of this study as the major benchmark to validate the data obtained by the GEM, especially the horizontal camera. The camera is composed by two arrays of 32 photo-diodes, spaced 50 mm apart, that generate a current when illuminated by the photons. The pinhole consists in a $1 \times 3\,\mathrm{mm}^2$ rectangular slit, equipped with a 12.5 μm thick Beryllium foil to stop low energy (< 1 keV) photons. The Line Of Sights (LOSs) are comparable to the GEM camera, as shown in figure 3.

The difference in LOSs between the GEM and the horizontal camera, particularly the smaller number of LOSs and plasma coverage of the GEM, is attributed to the compact design of the GEM diagnostic. This design facilitates easy orientation and positioning adjustments, including zooming in or out by moving the detector farther or closer to the pinhole. The radial orientation chosen for this experimental campaign enables a straightforward comparison with MAST-U horizontal camera data. However, future experimental campaigns will switch to a tangential orientation to fully exploit the bidimensionality of the camera, as demonstrated in [15].

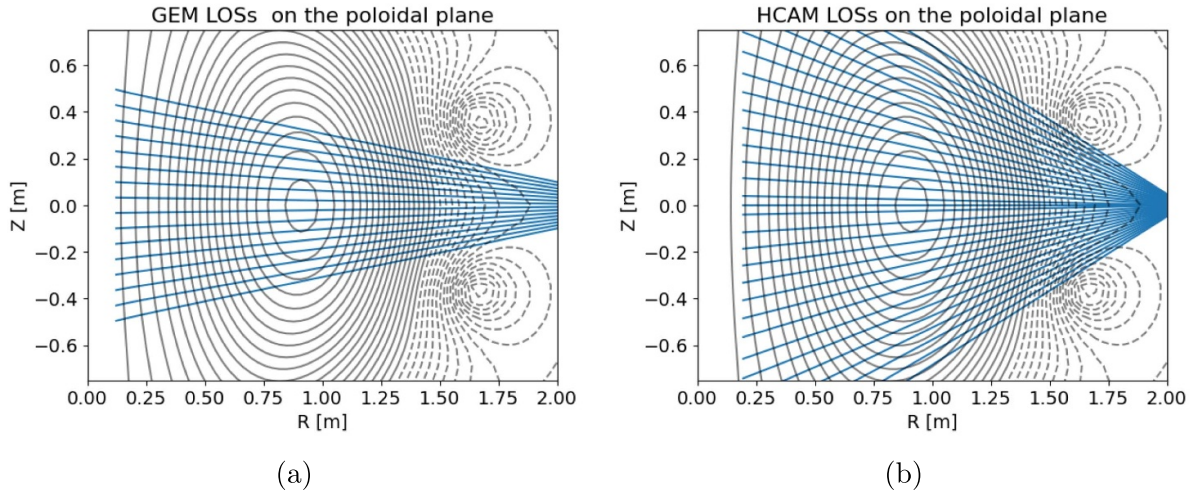

Figure 3. (a) LOSs geometry of the rows of the GEM camera. (b) LOSs geometry of the horizontal SXR camera.

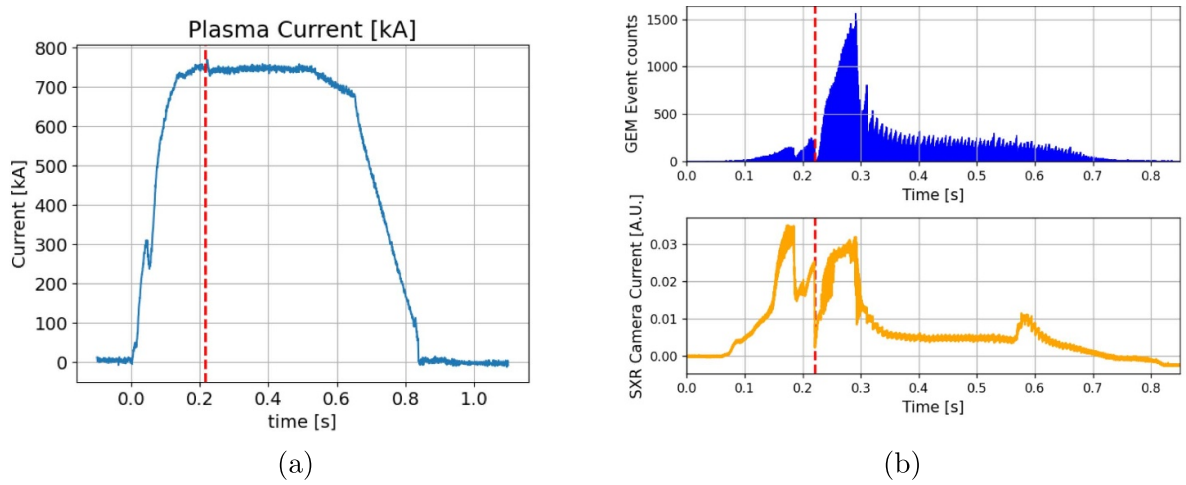

Figure 4. Ohmic shot #49020. (a) Plasma current. (b) Histogram of the GEM time-trace in blue on the upper plot, with a time binning of 0.1 ms; horizontal camera time-trace in orange on the lower plot. The IRE is highlighted with the dashed red line in the three graphs.

2. Data validation

In this section the first data from the GEM camera are presented and compared to the SXR horizontal camera data for validation.

The first comparison is made between the SXR signal time-trace of the core LOSs of the horizontal camera and the time-trace of the signal on the whole GEM camera (figure 4(a)); the Plasma Current signal of the same shot is shown in figure 4(b). The plots are obtained with different methods: the horizontal camera time-trace is a current signal over time of the diodes in the central region of the plasma, while the GEM time-trace is obtained as a time histogram of single event counts recorded by the detector over the pixels corresponding to the most central part of the plasma. Additional differences are that the sensitivity of a GEM detector is intrinsically different to the one of a diode, and the Beryllium foils thickness are different. The horizontal camera operates in the tokamak vacuum chamber, its Beryllium foil is 12.5 μm thick, thus the cut-off energy is 1 keV, and the diode sensitivity is constant in the SXR region. The GEM camera Beryllium foil instead is 25 μm and the photons path comprehend 30 cm of air, in which the Argon further attenuates the signal, summing up to an energy cut-off at 3.2 keV. The difference in the energy sensitivity can explain the data differences, such as the SXR radiation peak detected at 0.58 s by the horizontal camera, and not by the GEM camera. Nonetheless the key feature are present in both time-traces: the shot duration of 0.82 s, as well as the presence of a SXR crash at 0.21 s, (highlited by the red dashed line in figure) followed by a ramp in the SXR signal. The SXR crash is an effect the internal reconnection event (IRE), a phenomenon typical in Ohmic pulses of a ST [16], identified also with a spike in the plasma current. The presence of SXR signal peaks is similar in the two plots, while the heights are different because of different sensitivities.

Another interesting and key aspect of the SXR cameras is the spatial localization of the SXR activity. One example from the Ohmic shot #49020 is the localization of the peak of emission of a Snake instability [17, 18], whose fingerprint is shown in figure 5. This perturbation is characterized by a rotating

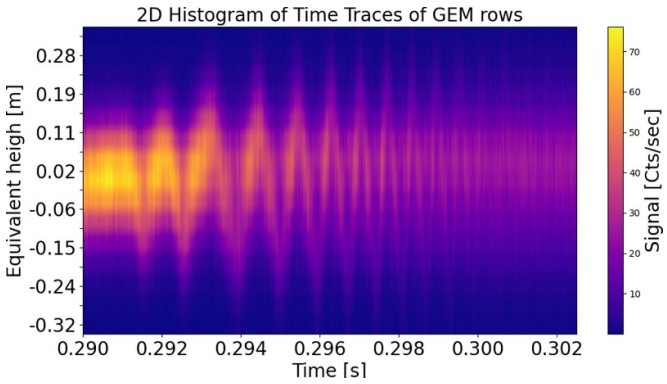

Figure 5. Ohmic shot #49020. The fingerprint of a snake instability, obtained by plotting the time histogram from every row of the GEM camera with a time binning of 10 μs. On the *y*-axis is shown the equivalent height: the height of each row LOS at the plasma axis.

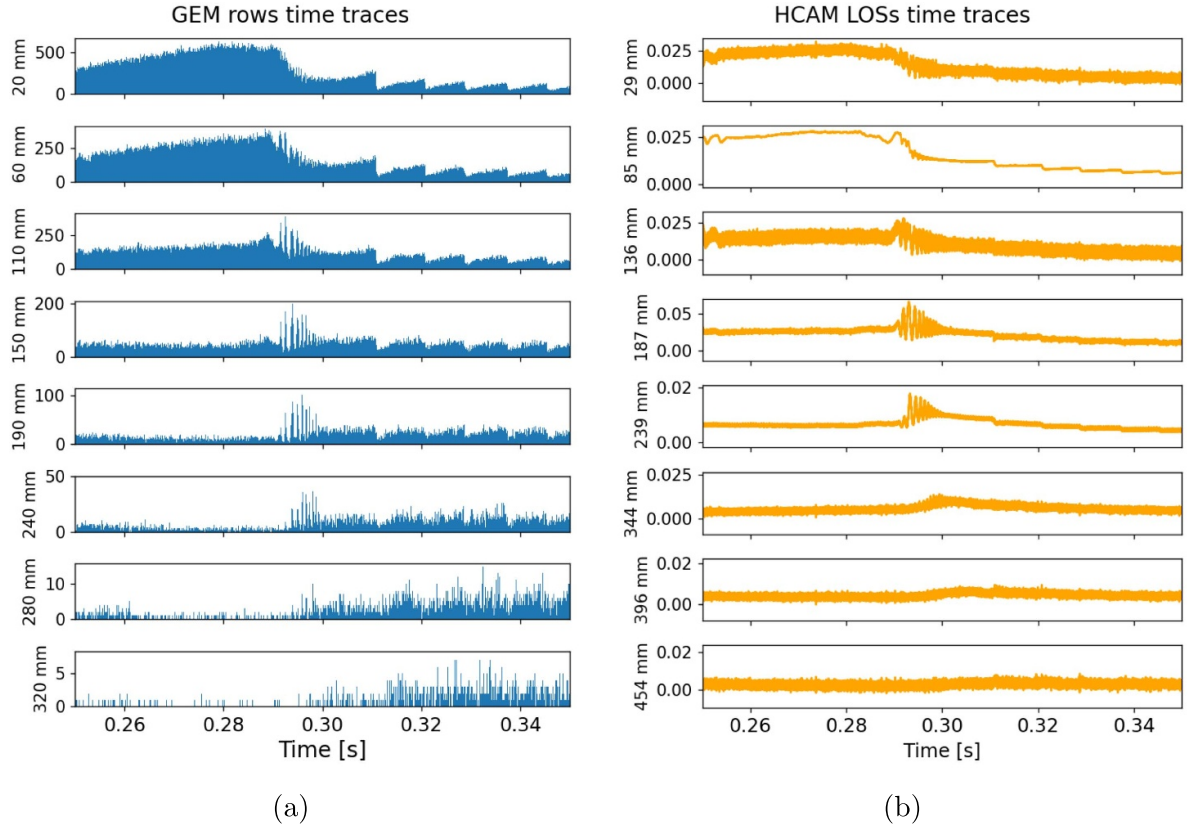

Figure 6. Ohmic shot #49020, presenting a snake instability at 0.29 s and the first sawtooth crash at 0.31 s. (a) Time-trace histogram for different GEM rows with 0.1 ms time binning, identified with their equivalent height (the height of each row LOS at the plasma axis). (b) Time-trace histogram for different horizontal camera LOSs, identified with their equivalent height.

region of high er density and enhanced x-ray emission, which is critical for monitoring the dynamic behavior of important plasma magnetic surfaces. In the MAST-U experiments, the observation of spontaneous snakes provides valuable insights into impurity accumulation and trapping in a magnetic island before the occurrence of the first sawtooth event [19], thereby enhancing our understanding of plasma behavior near these key surfaces. In the example presented, the first sawtooth crash occurs at 0.31 s, as illustrated in figure 6. The maximum extent of the peak of SXR emission on the z-axis is localized around ± 280 mm, according to both the GEM and the horizontal camera diagnostics, as shown in figure 6, where the emission peak is visible for the innermost LOSs and vanishes for the outermost (only half of the LOSs are shown for the sake of readability).

3. SXR energy

The primary contribution to SXR emission in a fusion plasma is from Bremsstrahlung radiation. The analytical formula describing the SXR emissivity ϵ, as a function of

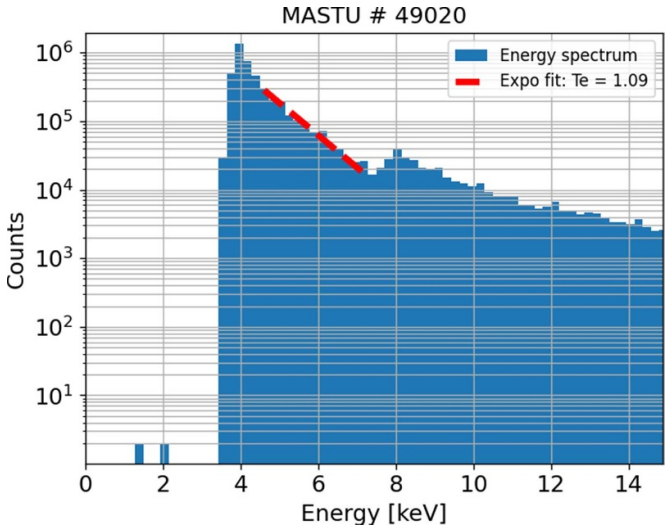

Figure 7. Ohmic shot #49020. Example of a GEM Energy spectrum integrate over the full pulse and over the entire camera. An exponential fit (the dashed red line) is applied in the range 4.2–7.5 keV to estimate the electron temperature, according to equation (2).

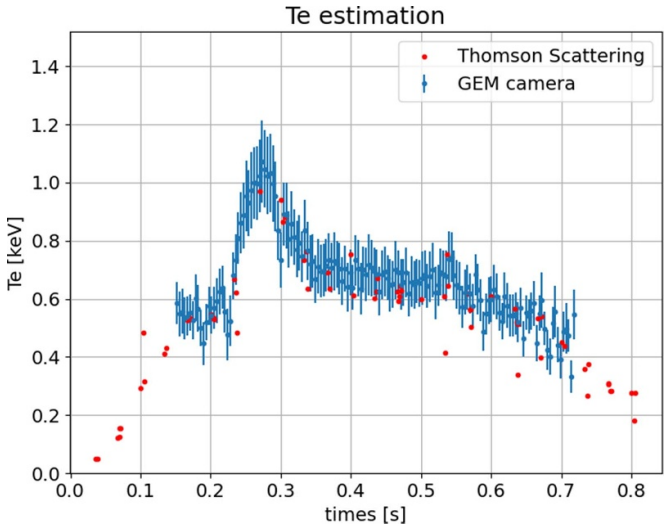

Figure 8. Ohmic shot #49020. Time evolution of the on-axis T_e obtained with the GEM camera (in blue) and with the TS diagnostic (in red).

tokamak major radius R and SXR energy E, exhibits a strong dependence on electron temperature (T_e) density (n_e) and effective ion charge (Z_{eff}); under the assumption of a Maxwellian plasma it shows an exponential decrease directly proportional to T_e [2]:

$$\epsilon(R,E) \propto E \cdot Z_{eff}(R) \cdot n_e^2(R) \cdot T_e^{-1/2} exp\left[\frac{-E}{k_B T_e(R)}\right] \quad (1)$$

The energy spectrum obtained by the GEM camera can provide significant information on plasma parameters by performing energy cuts or fitting to retrieve key parameters. An example is illustrated in figure 7: an exponential fit of the

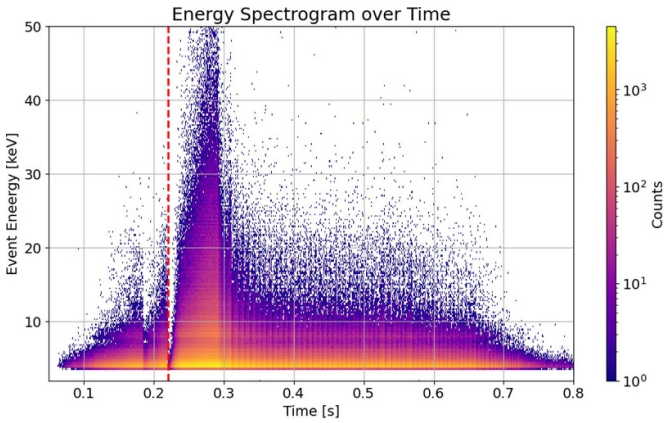

Figure 9. Ohmic shot #49020. Energy spectrogram: on the x-axis the time (time binning of 1 ms), on the y-axis the SXR energy in keV and the color proportional to the logarithmic number of events per bin.

equation (2), simplification of the equation (1), is used to directly determine T_e from the exponential coefficient

$$f(E) = A \cdot e^{-E/kT_e} \quad (2)$$

Two major assumptions underlie this approach: during the Ohmic shot, the plasma is assumed to be Maxwellian, and within the fitting interval, no additional features are present. The latter assumption restricts the fitting range at the low energy end to 4.2 keV, because the spectrum is affected by attenuation due to the Beryllium window and the air between the window and the detector. The upper limit is determined by the presence of a bump at 8 keV, the nature of which is not completely understood and will be investigated in future studies. Hypotheses include line emissions from plasma impurities or as a result of neutron background (topic discussed in section 4).

This analysis can be extended to spectra obtained in sequential time windows to monitor the evolution of T_e, and comparisons can be made with parameters obtained by the Thomson Scattering (TS) diagnostic present on MAST-U [20]. The comparison, as shown in figure 8, demonstrates good agreement despite the limitations of the simple method, indicating the potential for further refinement.

During the shot #49020, the IRE induces a loop voltage that accelerates ions and electrons, resulting in the burst of SXR emission (figure 6) and the rise of the T_e (figure 8). This event is also noteworthy from an energy spectrogram perspective (figure 9): the post-IRE burst generates a tail of supra-thermal electrons, in accordance with the theory [21]. However, the presence of a high-energy tail cannot be solely attributed to supra-thermal electrons, as the sensitivity of the GEM-based detector drops after 10 keV. This suggests the influence of neutron background, potentially indicating a rise in neutron yield coinciding with the increase in temperature. The subsequent section focuses on investigating the impact of the neutron field on the detector response.

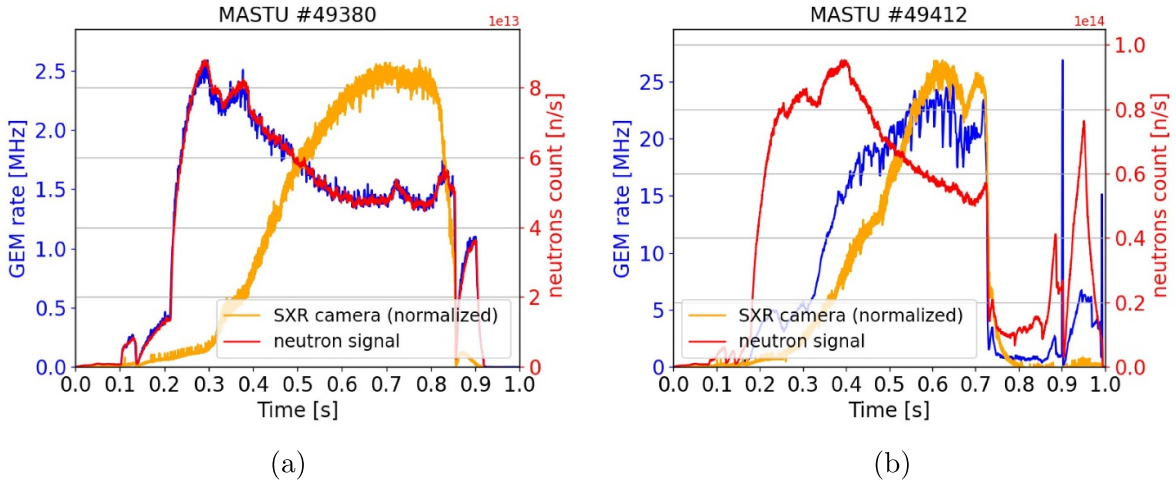

Figure 10. Comparison of the time evolution of: the GEM counts (in blue), the neutron rate (in red), normalized horizontal camera SXR signal (in orange) (a) Shot #49380, beam on, gate closed. (b) Shot #49412, beam on, gate open.

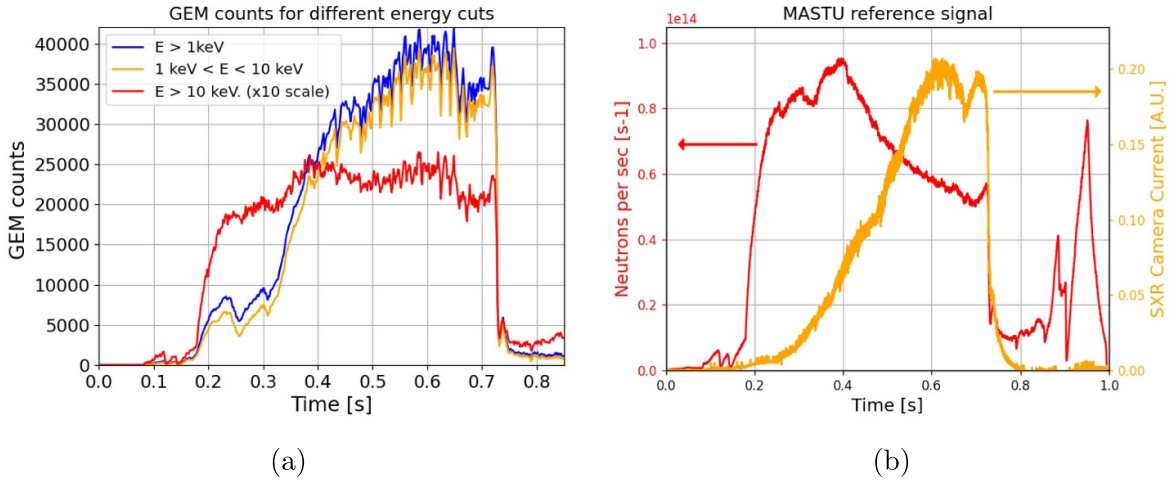

Figure 11. Signals time evolution of Shot #49412, with beam heating on. (a) GEM signal time trace. The global trace is shown in blue, the trace for events with energy $E < 10$ keV, in orange, and the trace for events with energy $E > 10$ keV, in red (scaled by a factor of 10 for visibility). (b) Reference signals: SXR time evolution in orange (referred to the y-axis on the right) and neutron rate time evolution in red (referred to the y-axis on the left).

4. Neutron background

To investigate the impact of neutron background on SXR detection the gate valve in front of the Beryllium window can be kept closed during selected MAST-U shots. In this configuration, SXR radiation is effectively blocked, allowing only neutrons and gammas to reach the GEM detector and produce signal [22]. Time-traces from these shots can then be compared with both the SXR signal from the horizontal camera and the signal from MAST-U neutron fission chambers [23], and compared to standard shots with the gate open. The data are presented in figure 10: the evolution of the GEM signal (in blue) closely resembles the neutron signal evolution (in red) in shots with the gate closed (figure 10(a)), whereas in shots with the gate open, it aligns with the horizontal camera signal (in orange, figure 10(b)). From this straightforward analysis, it is evident that there exists a neutron background in the GEM data.

Performing an energy cut on the GEM signal for shots with the gate open, as illustrated in figure 11, further confirms that the high-energy portion of the spectrum (i.e. events with energy > 10 keV, shown in red in figure 11(a)) is primarily attributed to neutron-related signals. Specifically, the high-energy signal closely mirrors the neutron signal (depicted in red in figure 11(b)), while the low-energy signal reproduces the SXR signal (represented by the orange lines in the figures). It is also noteworthy that the GEM global signal (in blue) continues to track the SXR evolution, and the ratio of counts indicates a neutron contribution ranging between 1% and 10% of the total signal, which varies with temporal

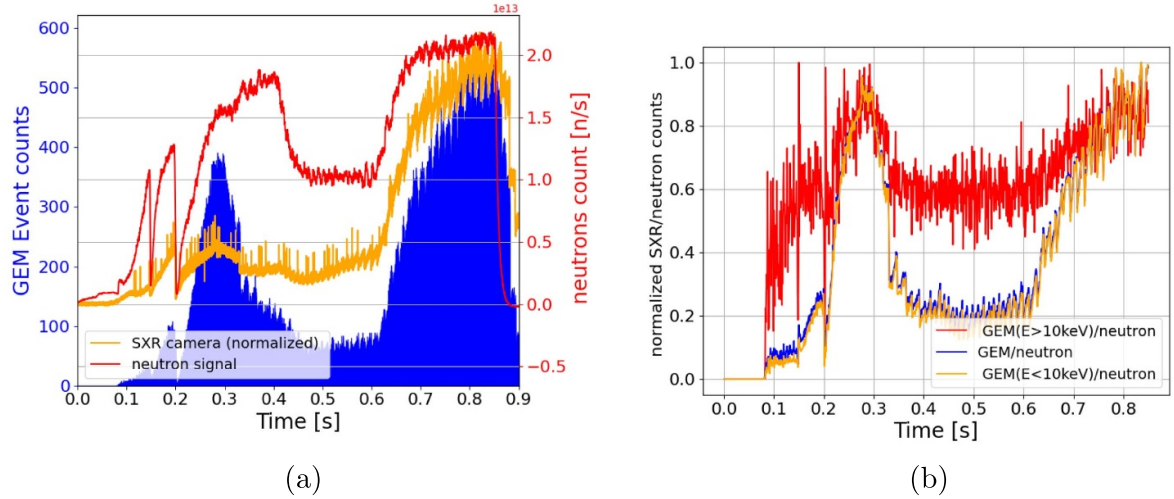

Figure 12. Beam heated Shot #49452. (a) GEM signal time-trace (in blue), normalized horizontal camera SXR signal (in orange), neutron rate evolution in time (in red). (b) Ratio of the GEM signal over the neutron rate signal for different energy cuts.

plasma parameters (higher during beam heated shots and lower during Ohmic shots, for instance) and the level of energy cut. This study highlights the need to enhance the signal to noise ratio (SNR) in order to perform finer energy analysis. The result can be achieved with two complementary design optimizations: switching the gas mixture from ArCO2 to NeCO2, because Neon is less sensitive to neutrons; and by filling the interspace between the GEM diagnostic and the external wall of the tokamak with an Helium buffer, in order to limit the abosrption of low energy SXR by air.

A final observation pertains to the post-IRE spike in the GEM signal discussed in section 3. It's worth understanding whether this spike is solely caused by an increase in neutron activity or by an increase in electron energy. Data from shot #49452 with neutral beam injection are analyzed in figure 12. The neutron rate rises sharply from 0.2 s to 0.3 s, and continues to grow at a slower pace until 0.4 s (shown in red in figure 12(a)). Meanwhile, the peak in the GEM time-trace occurs at 0.3 s, followed by a sharp decrease, as depicted by the blue line. Figure 12(b) displays the ratio of the GEM signal to the neutron rate for both the entirety of GEM events and a selection of events with energies smaller and greater than 10 keV. If the GEM signal were solely due to neutrons, as in the case of the gate-closed shots in figure 10(a), the plots would have been flat, showing data correlation. However, the peak observed between 0.2 s and 0.33 s in all three cases suggests that the signal is primarily due to SXR radiation, while the flatness between 0.33 s and 0.4 s indicates that the bump in the GEM signal is neutron-related. While precisely quantifying the signal components is not trivial and requires simulations and modeling, which will be performed in subsequent studies, a qualitative understanding can be obtained. The ratios of GEM signal over neutrons for different energy cuts show difference in the neutron contribution on the GEM signal. In fact the peaks at 0.28 s in the global and low-energy cut ratios (in blue and orange in figure 11(b)) are more prominent with respect to the one of the high energy cut (in red in figure 11(b)): the blue and orange peaks are roughly 4 times higher than the baseline, indicating a smaller neutron contribution, whereas in the high-energy cut ratio, the peak is only 1.5 times the baseline, suggesting that the neutron component on the high energy tail of the signal weights roughly three times more than on the lower side.

5. Conclusions and further developments

This work summarizes the investigation of the capabilities of a GEM-based diagnostic on a ST with radial line of sight. Through direct comparison with signals from the MAST-U SXR camera, the GEM data has been validated in terms of temporal trace and spatial analysis, demonstrating good agreement with the standard diagnostic set. Additionally, the GEM has shown potential for spectral analysis, yielding promising results for estimating plasma parameters and enabling offline energy cut on the signal.

The investigation into neutron background underscores the importance of optimizing the diagnostic to improve the SNR for clearer energy spectra and more precise energy analysis. To address this, the gas mixture in the GEM will be switched from ArCO2 to NeCO2, which exhibits lower sensitivity to neutrons. Furthermore, an He gas buffer will be installed in front of the camera, replacing the current air path, to limit the attenuation of low-energy SXR radiation and achieve a higher SNR.

Following the successful assessment confirming the diagnostic's capabilities, its orientation will be changed to a tangential line of sight to perform tomographic inversion of the signal and obtain 2D poloidal images of the emission.

Data availability statement

The data cannot be made publicly available upon publication because they are not available in a format that is sufficiently

accessible or reusable by other researchers. The data that support the findings of this study are available upon reasonable request from the authors.

Acknowledgments

This work has been carried out within the framework of the EUROfusion Consortium, funded by the European Union via the Euratom Research and Training Programme (Grant Agreement No. 101052200 EUROfusion) and from the EPSRC [Grant Number EP/W006839/1]. Views and opinions expressed are however those of the author(s) only and do not necessarily reflect those of the European Union or the European Commission. Neither the European Union nor the European Commission can be held responsible for them.

ORCID iDs

A Celora https://orcid.org/0009-0006-0160-2195
L Garzotti https://orcid.org/0000-0002-3796-9814
E Lazzaro https://orcid.org/0000-0002-3291-8890
D Rigamonti https://orcid.org/0000-0003-0183-0965
G Croci https://orcid.org/0009-0004-3302-4209

References

[1] Wesson J 2004 *Tokamaks* 3rd edn (Oxford University Press)
[2] Goeler S V, Stodiek W, Eubank H, Fishman H, Grebenshchikov S and Hinnov E 1975 Thermal x-ray spectra and impurities in the st tokamak *Nucl. Fusion* **15** 301
[3] Jardin A, Bielecki J, Mazon D, Dankowski J, Król K, Peysson Y and Scholz M 2020 Synthetic x-ray tomography diagnostics for tokamak plasmas *J. Fusion Energy* **39** 240–50
[4] Sauli F 2016 The gas electron multiplier (GEM): operating principles and applications *Nucl. Instrum. Methods Phys. Res.* A **805** 2–24
[5] Muraro A *et al* 2019 Development and characterization of a new soft x-ray diagnostic concept for tokamaks *J. Instrum.* **14** C08012
[6] Delgado-Aparicio L F *et al* 2007 High-efficiency fast scintillators for 'optical' soft x-ray arrays for laboratory plasma diagnostics *Appl. Opt.* **46** 6069–75
[7] Lee M, Kim J, Kim M, Lim S, Kim J and Sung C 2023 Development of a scintillator-based optical soft x-ray (OSXR) diagnostic system for kstar tokamak *Rev. Sci. Instrum.* **94** 053507
[8] Cordella F *et al* 2017 Results and performances of x-ray imaging GEM cameras on FTU (1-D), KSTAR (2-D) and progresses of future experimental set up on W7-X and EAST facilities *J. Instrum.* **12** C10006
[9] Mazon D *et al* 2022 First GEM measurements at WEST and perspectives for fast electrons and heavy impurities transport studies in tokamaks *J. Instrum.* **17** C01073
[10] Morris W, Harrison J, Kirk A, Lipschultz B, Militello F, Moulton D and Walkden N 2018 MAST upgrade divertor facility: a test bed for novel divertor solutions *IEEE Trans. Plasma Sci.* **46** 1217–26
[11] Caruggi F *et al* 2023 Performance of a triple GEM detector equipped with al-GEM foils for x-rays detection *Nucl. Instrum. Methods Phys. Res.* A **1047** 167855
[12] Pezzotta A, Corradi G, Croci G, Matteis M D, Murtas F, Tagnani D, Gorini G and Baschirotto A 2015 GEMINI, a CMOS 180 nm mixed-signal 16-channel ASIC for Triple-GEM detectors readout *2015 IEEE SENSORS–Proc.* p 12
[13] Cancelli S *et al* 2022 Electronic readout characterisation of a new soft x-ray diagnostic for burning plasma *J. Instrum.* **17** C08028
[14] Design of the FPGA-MB and of HVGEM Module, Gemini LNFWeb Site (available at: https://web.infn.it/GEMINI/)
[15] Qu H, Hu L, Cordella F, Claps G, Pacella D, Xu L and Li E 2019 Application of the Tikhonov tomography method for the gas electron multiplier (GEM) system on experimental advanced superconducting tokamak *Rev. Sci. Instrum.* **90** 093507
[16] Mizuguchi N, Hayashi T and Sato T 2000 Dynamics of spherical tokamak plasma on the internal reconnection event *Phys. Plasmas* **7** 940–9
[17] Weller A, Cheetham A D, Edwards A W, Gill R D, Gondhalekar A, Granetz R S, Snipes J and Wesson J A 1987 Persistent density perturbations at rational-q surfaces following pellet injection in the Joint European Torus *Phys. Rev. Lett.* **59** 2303–6
[18] Turri G, Buttery R, Cowley S, Gimblett C, Hastie R and Lehane I 2004 Magnetic reconnections in mast *31st EPS Conf. on Plasma Phys. London* vol 28
[19] Chapman I 2010 Controlling sawtooth oscillations in tokamak plasmas *Plasma Phys. Control. Fusion* **53** 013001
[20] Scannell R, Walsh M, Dunstan M, Figueiredo J, Naylor G, O'Gorman T, Shibaev S, Gibson K and Wilson H 2010 A 130 point ND: yag thomson scattering diagnostic on mast *Rev. Sci. Instrum.* **81** 10D520
[21] Helander P, Eriksson L-G, Akers R, Byrom C, Gimblett C and Tournianski M 2002 Ion acceleration during reconnection in MAST *Phys. Rev. Lett.* **89** 235002
[22] Esposito B, Marocco D, Villari R, Murtas F and Rodionov R 2014 Characterization of a GEM-based fast neutron detector *Nucl. Instrum. Methods Phys. Res.* A **741** 196–204
[23] Vincent C, Allan S, Naylor G, Stephen R, Bray S, Thornton A and Kirk A 2022 Fission chamber data acquisition system for neutron flux measurements on the Mega-Amp Spherical Tokamak Upgrade *Rev. Sci. Instrum.* **93** 093509